Video Article

High Precision FRET at Single-molecule Level for Biomolecule Structure Determination

Junyan Ma[1], Inna S. Yanez-Orozco[2], Soheila Rezaei Adariani[2], Drew Dolino[3], Vasanthi Jayaraman[3], Hugo Sanabria[2]

[1]Department of Chemistry, Clemson University

[2]Department of Physics and Astronomy, Clemson University

[3]Department of Biochemistry and Molecular Biology, Center for Membrane Biology, Graduate School for Biomedical Sciences, University of Texas Health Science Center

Correspondence to: Hugo Sanabria at hsanabr@clemson.edu

URL: https://www.jove.com/video/55623
DOI: doi:10.3791/55623

Keywords: Biochemistry, Issue 123, FRET, single molecule, interdye distance, DNA, fluorophore, multiparameter fluorescence detection, pulsed interleaved excitation, protein labeling

Date Published: 5/13/2017

Citation: Ma, J., Yanez-Orozco, I.S., Rezaei Adariani, S., Dolino, D., Jayaraman, V., Sanabria, H. High Precision FRET at Single-molecule Level for Biomolecule Structure Determination. *J. Vis. Exp.* (123), e55623, doi:10.3791/55623 (2017).

Abstract

A protocol on how to perform high-precision interdye distance measurements using Förster resonance energy transfer (FRET) at the single-molecule level in multiparameter fluorescence detection (MFD) mode is presented here. MFD maximizes the usage of all "dimensions" of fluorescence to reduce photophysical and experimental artifacts and allows for the measurement of interdye distance with an accuracy up to ~1 Å in rigid biomolecules. This method was used to identify three conformational states of the ligand-binding domain of the N-methyl-D-aspartate (NMDA) receptor to explain the activation of the receptor upon ligand binding. When comparing the known crystallographic structures with experimental measurements, they agreed within less than 3 Å for more dynamic biomolecules. Gathering a set of distance restraints that covers the entire dimensionality of the biomolecules would make it possible to provide a structural model of dynamic biomolecules.

Video Link

The video component of this article can be found at https://www.jove.com/video/55623/

Introduction

A fundamental goal of structural biology studies is to unravel the relationship between the structure and function of biomolecular machines. The first visual impression of biomolecules (*e.g.,* proteins and nucleic acids) occurred in the 1950s through the development X-ray crystallography[1,2]. X-ray crystallography provides high-resolution, static structural information constrained by the crystal packing. Therefore, the inherent immobility of X-ray structural models shuns the dynamic nature of biomolecules, a factor that impacts most biological functions[3,4,5]. Nuclear magnetic resonance (NMR)[6,7,8] provided an alternative solution to the problem by resolving structural models in aqueous solutions. A great advantage of NMR is its ability to recover the intrinsic dynamic nature of biomolecules and conformational ensembles, which helps to clarify the intrinsic relationships between structure, dynamics, and function[3,4,5]. Nevertheless, NMR, limited by sample size and large amounts of sample, requires complex labeling strategies for larger systems. Therefore, there is a pressing need to develop alternative methods in structural biology.

Historically, Förster resonance energy transfer (FRET)[9] has not taken an important role in structural biology because of the misconception that FRET provides low-accuracy distance measurements. It is the purpose of this protocol to revisit the ability of FRET to determine distances on the nanometer scale, such that these distances can be used for building structural models of biomolecules. The first experimental verification of the R^{-6} dependence on the FRET efficiency was done by Stryer in 1967[10] by measuring polyprolines of various lengths as a "spectroscopic ruler." A similar experiment was accomplished at the single-molecule level in 2005[11]. Polyproline molecules turned out to be non-ideal, and thus, double-stranded DNA molecules were later used[12]. This opened the window for precise distance measurements and the idea of using FRET to identify structural properties of biomolecules.

FRET is optimal when the interdye distance range is from ~0.6-1.3 R_0, where R_0 is the Förster distance. For typical fluorophores used in single-molecule FRET experiments, R_0 is ~50 Å. Typically, FRET offers many advantages over other methods in its ability to resolve and differentiate the structures and dynamics in heterogeneous systems: (i) Due to the ultimate sensitivity of fluorescence, single-molecule FRET experiments[13,14,15,16] can resolve heterogeneous ensembles by directly counting and simultaneously characterizing the structures of its individual members. (ii) Complex reaction pathways can be directly deciphered in single-molecule FRET studies because no synchronization of an ensemble is needed. (iii) FRET can access a wide range of temporal domains that span over 10 decades in time, covering a wide variety of biologically relevant dynamics. (iv) FRET experiments can be performed in any solution conditions, *in vitro* as well as *in vivo*. The combination of FRET with fluorescence microscopy allows for the study of molecular structures and interactions directly in living cells[15,16,17,18,19], even with high precision[20]. (v) FRET can be applied to systems of nearly any size (*e.g.,* polyproline oligomers[21,22,23,24], Hsp90[25], HIV reverse transcriptase[26], and ribosomes[27]). (vi) Finally, a network of distances that contains all the dimensionality of biomolecules could be used to derive structural models of static or dynamic molecules[18,28,29,30,31,32,33,34,35,36,37].

Therefore, single-molecule FRET spectroscopy can be used to derive distances that are precise enough to be used for distance-restrained structural modeling[26]. This is possible by taking advantage of multiparameter fluorescence detection (MFD)[28,38,39,40,41,42], which utilizes eight dimensions of fluorescence information (*i.e.,* excitation spectrum, fluorescence spectrum, anisotropy, fluorescence lifetime, fluorescence quantum yield, macroscopic time, the fluorescence intensities, and the distance between fluorophores) to accurately and precisely provide distance restraints. Additionally, pulsed interleaved excitation (PIE) is combined with MFD (PIE-MFD)[42] to monitor direct excitation acceptor fluorescence and to select single-molecule events arising from samples containing a 1:1 donor-to-acceptor stoichiometry. A typical PIE-MFD setup uses two-pulsed interleaved excitation lasers connected to a confocal microscope body, where photon detection is split into four different channels in different spectral windows and polarization characteristics. More details can be found in **Figure 1**.

It is important to note that FRET must be combined with computational methods to achieve atomistic-like structural models that are consistent with FRET results[26,30]. It is not the goal of the present protocol to go over the associated methodology to build structural models with FRET-derived distances. However, these approaches have been applied in combination with other techniques (*e.g.,* small-angle X-ray scattering or electron paramagnetic resonance), giving birth to the field of integrative structural biology[43,44,45,46]. The current goal is to pave the way for FRET as a quantitative tool in structural biology. As an example, this methodology was used to identify three conformational states in the ligand-binding domain (LBD) of the N-methyl-D-aspartate (NMDA) receptor. The ultimate aim is to overcome the aforementioned limitations and to bring FRET amongst the integrative methods used for the structural determination of biomolecules by providing measured distances with high precision.

Protocol

1. PBS Buffer Preparation and Chamber Treatment

NOTE: Wear a laboratory coat and disposable gloves when performing wet chemical experiments. Use eye protection when aligning the laser.

1. **PBS buffer preparation**
    1. Dissolve 4.5 g of Na_2HPO_4, 0.44 g of NaH_2PO_4, and 3.5 g of NaCl in 400 mL of distilled water. Ensure a pH of 7.5 and sterilize the solution by autoclaving on a liquid cycle for 1 h (depending on the autoclave system).
    2. Take 15 mL of the PBS solution and mix it with 0.1 g of charcoal. Filter the mix by using a regular 20 mL syringe filter with a 0.2 µm pore **size. Seal and store the PBS buffer at room temperature.**

2. **Microscope chambered cover glass treatment**
    1. Add 500 µL of distilled water and 5 µL of polysorbate 20 nonionic surfactant (see the Materials List) to a chambered cover glass system (see the Materials List) and mix well. Let it soak for 30 min. Remove the polysorbate 20 solution and wash the chamber with distilled water twice. Let it dry.
    NOTE: The chamber is now ready to use.

2. DNA Sample Preparation

NOTE: Use designed labeled DNA strands (see the Materials List) for the creation of double-stranded DNA (dsDNA) standard samples. Designed oligos must not have dyes at the end of a polymer in order to avoid artifacts that can compromise the determined distance. The DNA sequence should be chosen to behave as a rigid body.

1. Add 1.5 µL of a donor labeled DNA strand and 4.5 µL of a complimentary (acceptor-labeled or non-labeled) DNA strand into a microfuge tube and mix them with 24 µL of nuclease-free water.
NOTE: Depending on the mix of the selected oligonucleotides, the following samples will be generated: no-FRET, low-FRET, or high-FRET dsDNAs.
2. Hybridize the DNA using a thermal mixer and the following process: 95 °C for 10 min, 90 °C for 10 min, 80 °C for 10 min, 70 °C for 10 min, 60 °C for 10 min, 50 °C for 10 min, 40 °C for 10 min, 30 °C for 10 min, 20 °C for 10 min, 10 °C for 10 min, and holding at 5 °C.
NOTE: The generated dsDNA standards can be kept in a -20 °C freezer for long-term storage or can be used immediately.

3. Protein Sample Preparation

Note: Starting with recombinant DNA for the expression of the protein of interest in bacterial systems, it is possible to mutate the residues from which the distances are to be measured into cysteines. To do so, use standard site-directed mutagenesis techniques[47]. To facilitate protein purification, clone the recombinant and mutated DNA into a vector containing a purification tag (*e.g.,* a His-tag). The glutamate subunit 1 ligand-binding domain (LBD) from the NMDA glutamate ionotropic receptor (GluN1) LBD (*i.e.,* NMDA GluN1 LBD cloned into the pET-22b (+) vector) was used.

1. **Protein expression**
    1. Transform construct DNA plasmid into the expression system of choice[48].
    NOTE: The following steps will assume that the expression of a soluble protein is transformed in *Escherichia coli*. Purification from, for example, transfected mammalian cells[49] or transduced insect cells[50], is also possible, and detailed steps can be found elsewhere. Ensure that the *E. coli* strain selected is appropriate for the protein of interest. For example, the expression of proteins that contain disulfide bridges requires a strain of competent cells with a less-reducing intracellular compartment (see the Materials List).
    2. Inoculate a starter *E. coli* culture by using a sterile pipette tip to pick up a single transformed colony[48]. Drop it into 100 mL of selective LB medium (see the Materials List) and allow the culture to grow overnight at 37 °C.
    3. Prepare LB broth (see the Materials List). Autoclave it to sterilize.
    4. Inoculate large-scale cultures of transformed *E. coli* by adding the overnight culture to 2 L of selective LB medium at a 1:500 ratio.

5. Over the next few hours, assess the growth of the culture by monitoring the absorbance readings (Abs) of the culture at 600 nm, sometimes referred to as the optical density at 600 nm (OD_{600}), or by using a cell density meter. Note that the readings increase over time.
6. Induce protein expression with a final concentration of 0.5 mM isopropyl-β-d-1-thiogalactopyranoside (IPTG) when the culture reaches an OD_{600} of 0.7. Shake induced *E. coli* at 20 °C for 20-24 h.
7. After protein induction, pellet the *E. coli* by spinning for 20 min at 3,000 x g and 4 °C. Discard the supernatant and store the *E. coli* pellet containing the intracellular protein at -80 °C until use.

2. **Protein purification**
   1. Lyse *E. coli* using a lysis method of choice (*e.g.,* sonication, French press, nitrogen cavitation, *etc.*)[51].
   2. Spin down the membrane and cell debris by centrifuging the lysate for 1 h at 185,000 x g and 4 °C.
   3. For a His-tagged protein, load the supernatant onto an equilibrated, nickel-charged, immobilized metal affinity chromatography (IMAC) column using a fast protein liquid chromatography (FPLC) system (see the **Materials Table**)[52].
      NOTE: Equilibration buffer for the NMDA GluN1 LBD: 200 mM NaCl, 20 mM Tris, and 1 mM Glycine, pH 8. Elution buffer for NMDA GluN1 LBD: 200 mM NaCl, 20 mM Tris, 1 mM Glycine, and 400 mM Imidazole, pH 8.
      1. Wash the IMAC column with buffer containing a low amount (~12 mM) of imidazole.
      2. Elute the protein from the IMAC column using a linear gradient of imidazole from 12 mM to 400 mM.
   4. Dialyze the protein overnight in equilibration buffer without imidazole[53] by placing the eluate from step 3.2.3.2 into dialysis tubing and submerging it in the equilibration buffer under continuous stirring for 2-3 h. Repeat at least one more time.
      NOTE: Steps 3.2.3-3.2.6 assume the purification of a His-tagged protein. If purifying through some other method, adjust the protocol accordingly.
   5. Quantify the protein amount by taking the absorbance at 280 nm of the dialyzed protein and using Beer's Law (*Absorbance unit* = ε *L c*, where ε is the extinction coefficient ($M^{-1}cm^{-1}$), which can be obtained here[54]; *L* is the light path length (cm); and *c* is the protein concentration (M)).
      NOTE: Various protein quantification assays are available, including the Bradford assay and bicinchoninic acid assay. Both provide accurate results.

3. **Protein labeling**
   1. Add donor (maleimide reactive cyan-green dye) and acceptor (maleimide reactive far-red dye) fluorophores to the purified protein at a 1:1:8 protein:donor:acceptor molar ratio.
   2. Incubate the protein and fluorophore mixture on ice for 30 min. Longer incubation times are possible.
   3. Pack a 0.5 mL Ni-Nitrilotriacetic acid (Ni-NTA) agarose column (see the Materials List) and equilibrate it using the same equilibration buffer as in step 3.2.3 while the protein is incubating.
      NOTE: Keep the amount of loaded protein in accordance with the resin binding capacity.
   4. After the 30 min incubation, load the protein/fluorophore mixture onto the column prepared in step 3.3.3 and purify by gravity flow.
   5. Wash off excess fluorophore with 5 mL of equilibration buffer.
   6. Elute the labeled protein by gravity from the column four times with 0.5 mL of elution buffer. Because the protein has already been purified from other proteins, no gradient is necessary.
   7. Check each eluate with a UV-Vis spectrometer to identify which fraction contains the labeled protein. Scan the absorbance from 230-700 nm to be able to ensure that the absorbance peaks from the protein (280 nm) and each fluorophore (493 nm for the cyan-green fluorophore and 651 nm for the far-red fluorophore) are visible in the eluate.
      NOTE: Typically, the protein will elute in fraction 2.
   8. Equilibrate a desalting column (see the **Materials Table**) with charcoal-treated PBS (step 1.1).
   9. Load the labeled protein onto the desalting column by gravity flow.
      NOTE: Keep the amount of loaded protein in accordance with the selected desalting column capacity[55].
   10. Elute using 3.5 mL of charcoal-treated PBS by gravity flow and collect 0.5 mL fractions of the eluate.
   11. Use a UV-Vis spectrometer to scan the absorbance of each eluate from 230-700 nm to identify which fraction contains labeled protein.
      NOTE: Steps 3.3.8-3.3.11 basically serve as a buffer exchange step. Other protocols that serve this purpose are also possible (*e.g.,* extensive dialysis). Alternatively, one could go straight to step 3.3.8 from step 3.3.2.

4. Measurements Needed in Ensemble Conditions (in Cuvette)

1. **Determination of the Förster constant**
   1. Scan f_D, the fluorophore fluorescence emission (cps), in a fluorimeter by exciting the donor at 15 nm to its maximum absorbance wavelength in order to get the full emission spectrum. Monitor the emission beginning 5 nm after the excitation wavelength and ending 150 nm later. Use magic angle conditions by setting the emission polarizer to 54.7° and the excitation polarizers to 0°[56].
      NOTE: For the donor fluorophore used here, the Abs maximum occurs at 490 nm; 475 nm is used as the excitation wavelength, and the emission from 480-650 nm is monitored. For the acceptor, the Abs maximum occurs at 645 nm; 630 nm is used for the excitation wavelength, and the emission from 635-735 nm is monitored.
   2. Use the fluorimeter to perform an excitation scan of the acceptor fluorophore (Abs_A) ranging from 400-700 nm and use magic angle conditions by setting the emission polarizer to 54.7° and the excitation polarizers to 0°[56]. Set the emission monochromator to 15 nm after the maximum-emission wavelength. Normalize to the maximum excitation value.
   3. On published tables, locate the extinction coefficient of the acceptor, ε_A (M^{-1} cm^{-1})[56], or use values provided by the manufacturer.
      NOTE: The value published for the acceptor fluorophore used in this manuscript is ε_{A647} = 270,000 cm^{-1} M^{-1} [56].
   4. Calculate the spectral overlap using $J = \Sigma f_D \cdot (Abs_A \cdot \varepsilon_A) \cdot \lambda^4$, where f_D, Abs_A, and ε_A have been defined above λ and is the wavelength (nm). Use a worksheet to list in columns all the wavelength-dependent values obtained in steps 4.1.1-4.1.3. Align them according to wavelength. Perform the summation from the minimum wavelength of the donor emission (λ_{min}) to the maximum wavelength of the acceptor absorbance (λ_{max}).

5. Calculate the Förster constant (R_o) using the following formula $R_o^6 = 8.79 \times 10^{-5} \cdot J \cdot \kappa^2 \cdot \Phi_{F,D} \cdot n^{-4}$, where J is the spectral overlap previously calculated in step 4.1.4, κ^2 is the orientation factor, $\Phi_{F,D}$ is the fluorescence quantum yield of the donor fluorophore, and n is the refractive index of the medium in which the fluorophore is situated.
   NOTE: Use n = 1.33 (if aqueous buffer is used) and $\kappa^2 = 2/3$.
6. Locate the quantum yield value of the donor fluorophore ($\Phi_{F,D}$, environment dependent) on published tables (see Reference 57) and use the value of the spectral overlap obtained in step 4.1.4 to calculate the final value of the Förster constant using the equation from step 4.1.5.
   NOTE: If the quantum yield is not available, follow step 4.2, below, to calculate it. In this case, use $\Phi_{F,D} = 0.8$, which corresponds to a donor lifetime $\tau_{D,r} = 4.0$ ns.

2. **Determination of fluorescence quantum yield**
   NOTE: The following procedure assumes only dynamic quenching. To consider static quenching, refer to Reference 56. However, PIE-MFD experiments are also useful in determining the quantum yield, even in the case of static quenching (see the Results).
   1. Select a reference fluorophore with similar absorbance and emission profiles for both the acceptor and the donor fluorophores for which the quantum yield (Φ_r) has been determined.
      NOTE: For the donor, $\Phi_r = 0.8$ and $\tau_r = 4$ ns, while for the acceptor, $\Phi_r = 0.32$ and $\tau_r = 1.17$ ns, which correspond to the Φ_r and τ_r for the cyan-green fluorophore- and the far-red fluorophore-labeled oligonucleotides, respectively[57].
   2. Measure the time-resolved fluorescence decay (f(t)) using the time-correlated single-photon counting (TCSPC) method at magic-angle conditions.
   3. Fit the fluorescence decay with a mono- or multi-exponential decay function in the form of $f(t) = \Sigma_i x_i e^{-t/\tau_i}$, where x_i is the population fraction and τ_i is the population fluorescence lifetime.
   4. Calculate the species average lifetimes, $\#\tau\#_x = \Sigma x_i \tau_i$, where x_i is the population fraction and τ_i is the population fluorescence lifetime.
   5. Use the formula $\Phi_{F,D} = \#\tau_D\#_x * \Phi_r / \tau_r$ to calculate the fluorescence quantum yield of the donor fluorophore by plugging in the fluorescence lifetime and quantum yield of the reference, as well as the fluorescence lifetime of the donor fluorophore.
      NOTE: This method assumes dynamic quenching. For other $\Phi_{F,D}$ determinations, follow Lakowicz[56].

5. Experiment Alignment for PIE-MFD Single-molecule Detection (SMD)

NOTE: It is better to turn off the lights when taking measurements.

1. **Equipment adjustment (Figure 1)**
   NOTE: A home-built MFD setup depicted in **Figure 1**, with two pulsed lasers and 4 detection channels in an inverted microscope body, is used for this experiment. There are similar commercial systems.
   1. Turn on the 485-nm and 640-nm lasers and all detectors of the MFD setup. Open the software that controls the TCSPC acquisition and lasers. Make sure that the laser repetition rate is 40 MHz.
   2. Set the 485-nm pulsed laser power to 60 µW at an image plane of the 60X 1.2 N.A. water-immersion objective and the 640-nm pulsed laser power to 23 µW in pulsed interleaved excitation mode (PIE-MFD)[42].
      NOTE: To set PIE-MFD, the two laser pulses are delayed in the laser controller software. For 485-nm laser excitation, the detection TCSPC channels (TAC channels) are 1-12,499 ("prompt" channel). For 640 nm laser excitation, the detection TCSPC channels (TAC channels) are 12,499-50,000 ("delay" channel).
   3. Add objective immersion liquid (a drop of double-distilled water) between the microscope objective lens and a cover glass slide. To ensure that the image plane is inside the solution and far from the glass surface, turn the adjustment knob one and a half turns after finding the second bright focal point due to the reflection of the lasers at the glass-liquid interface.
   4. Add 1 µL of 100 nM Rhodamine 110 to 50 µL of distilled water to the center of the cover glass. Ensure that the solution is also at the center of the microscope objective.
   5. Adjust the pinhole (size: 70 µm) positions (x and y direction one at a time) while monitoring the photon count rate on the acquisition software to maximize the number of photons detected.

2. **Standard measurement SMD (work in a dark room)**
   1. Use the sample from step 5.1.4 and record 120 s of the count rate by clicking the "Start" button on the time-tagged time-resolved (TTTR) control panel in "*.ht3" format[58] on the acquisition software.
   2. Compute offline fluorescence correlation spectroscopy (FCS)[59,60,61] (*i.e.,* FCS measurement) to determine the characteristic time of diffusion, the number of molecules in the confocal volume, the triplet state kinetics, and the molecular brightness[62].
      1. Open the software for FCS (Kristine, MFD suite). Select the experimental settings by clicking "Options" -> "Select Set up." Select a file with similar experimental settings and click "get parameters from file" to read the header information on the file.
      2. Select "Operate" -> "Correlate" to perform FCS.
         NOTE: Make sure that the channel numbers are properly specified and that the "TAC Gate" (TCSPC channels) is checked to select accordingly the prompt or delay channels.
      3. Select "Operate" -> "Global Fit of Correlation Curves" to open the fit routine. Use "equation #24" on the software and click "start."
         NOTE: Equation #24 on the software describes the autocorrelation function (G_c) of freely diffusing fluorescent molecules over a three-dimensional Gaussian illumination profile, such as[61]:

$$G(t_c) = 1 + \frac{1}{N(1-x_T)} \frac{1}{1+\frac{t_c}{t_{diff}}} \frac{1}{\sqrt{1+(\omega^2)\frac{t_c}{t_{diff}}}}$$

         where *N* is the mean number of molecules in the detection volume, x_T is the fraction of molecules exerting triplet-state kinetics with the characteristic time t_T, t_c, is the correlation time, t_{diff} is the diffusion time related to the geometrical parameter ω, and

ω describes the Gaussian illumination profile. After the fit, take note of the diffusion time and the number of molecules in the confocal volume.

3. Add 10 µL of 100 nM Rhodamine 101 into 50 µL of distilled water and mix well. Place this mix on top of the cover glass and ensure that the droplet is at the center of the objective lens. Click the "start" button on the TTTR control panel to record 120 s of data in TTTR format.
4. Add 1 µL of 100 nM far-red fluorophore into 50 µL of distilled water and mix well. Place this mix at the center of the objective lens. Click the "Start" button and record 120 s of data in TTTR format.
5. Place 50 µL of distilled water at the center of the objective lens. Click the "Start" button and record 300 s of data in TTTR format.
6. Place 50 µL of PBS buffer at the center of the objective lens. Click the "Start" button and record 300 s of data in TTTR format.
7. Take 1 µL of the mix from step 5.1.4 and mix with 50 µL of distilled water. Place this mix on the cover glass. First, click the "Start" button and collect 10 s of data in TTTR mode. Then, analyze the TTTR mode file using the Burst Integration Fluorescence Lifetime (BIFL) analysis software (Paris, MFD suite), as described in step 5.3.
   NOTE: Verify the number of bursts per second from the burst selection and analysis software[26,61]. If the burst level is around 35 every 10 s, it is appropriate for single-molecule measurement.
8. Continue recording the count rate in TTTR format for 1.5 h (*i.e.,* TCSPC at SMD) to treat as a single-molecule measurement standard.
   NOTE: Due to the large file size, split raw "*.ht3" files into smaller-size files to load and process using BIFL.

3. **Analysis of standard samples using BIFL**
   1. Open the BIFL software (Paris).
   2. Select the setup for PIE in the "confirm set up" automatic pop-up window and read the header by selecting the file with similar experimental settings. Click "get parameters from file." Click "OK." Note that the pop-up window closes and is integrated into the Paris front-end. Click "OK" under "Next."
   3. Choose the files to analyze by clicking "Select" on "Data Path Array" to select the measurement to analyze.
      1. Click on "Green scatter" (for a water measurement), "Green BG" (for a buffer measurement), "Green thick" (for a 2 nM Rhodamine 110 measurement), "Red scatter" (for a water measurement), "Red BG" (for a buffer or water measurement), "Red thick" (for a 20-nM Rhodamine 101 measurement), "Yellow scatter" (for a water measurement), "Yellow BG" (for a buffer measurement), and "Yellow Thick" (for a 2 nM far-red fluorophore measurement).
      2. Click "OK" under "Next."
         NOTE: The "Green" channel corresponds to the signal of the green detectors in the "prompt" TCSPC channels. The "Red" channel corresponds to the signal of the red detectors in the "prompt" TCSCP channels. The "Yellow" channel corresponds to the signal of the red detectors in the delay TCSPC channels.
   4. Click "Adjust" next to "Data cut Burstwise" to adjust single-molecule selection parameters. In the new pop up window, select single-molecule events with two standard deviations from the mean interphoton arrival time ("dt") by changing the interphoton arrival time under "Threshold" and the minimum number of photons per single molecule event under "min. #." Click "Return" to close the pop-up window. Click "OK" under "Next."
      NOTE: The threshold, in ms units, depends on the background count rate. The typical minimum number of photons used is 60.
   5. Adjust the initial fluorescence lifetime "Color fit parameters" (*e.g.*, from, to, and convolution) for the generated fluorescence decay parameters on the "Green", "Red," and "Yellow" colors. In the same window, adjust the "from" and "to" values for "Prompt" and "Delay." Click "Return" to close the pop-up window. Click "OK" under "Next."
      NOTE: Ensure that the 2-color excitation check-box is selected. "From" and "to" correspond to the initial and end bins on the fluorescence decay histogram (TAC channel number). If the initial fit parameters are selected properly, a fit function is added to the fluorescence decays on each channel.
   6. Select the location on the hard drive to which to save all processed ascii files in a parent folder.
      NOTE: Paris processes all selected bursts and creates multiple ascii output files than can be used by other programs for visualization (*e.g.,* Margarita MFD suite).

6. dsDNA Standards and Sample Measurements

1. Add 500 µL of PBS buffer to a chambered cover glass and place a drop of distilled water between the chamber and the objective lens. Click the "Start" button on the control pedal and collect 5 min of data in TTTR mode to use for analysis.
2. Take a small amount (usually around 0.1 µL, concentration of around 1 µM) of dsDNA standard, add it to the PBS buffer, and mix well. First, collect 10 s of data by clicking "Start." Then, check the burst to get 35 bursts per 10 s (as in steps 5.2.7 and 5.3). Finally, collect >2 h of data in TTTR format, as described above.
3. Analyze the collected data for the dsDNA samples, as in step 5.3.3.
4. **Visualize the burst histograms using the MFD suite (Margarita) and display the FRET efficiency versus $\#\tau_{D(A)}\#_f$ or the F_D/F_A versus $\#\tau_{D(A)}\#_f$.**
   1. Open the Margarita software and select "File" -> "Import all *.??4 and *.mti files." Select the parent folder containing various subfolders.
   2. Select the parameters to visualize by clicking next to the "X" (abscissa) of one of the parameters derived from Paris (*e.g.,* tau green or $\#\tau_{D(A)}\#_f$); similarly, repeat this for the ordinate "Y" to select the desired parameter to visualize (*e.g.,* FRET efficiency, F_D/F_A, or S_{PIE} PIE).
      NOTE: In this case, FRET efficiency, F_D/F_A, or S_{PIE} correct for proper background count rate in the green, red, and yellow channels; for quantum yields of the donor and acceptor; for the detection efficiency ratio (g_G/g_R); and for crosstalk (α). Here, g_G/g_R = 3.7 and α = 0.017, depending only on the instrument. Background count rates depend on the buffer used, and quantum yield values are previously determined.
   3. Add a FRET line by opening the "Overlay Equation" window by clicking "Display" -> "Overlay Equation." Select the static FRET line from the pop-up menu. Select the proper donor lifetimes and quantum yield parameters to generate the proper FRET line.

NOTE: FRET lines for correlating various FRET indicators can be generated.

5. Determine the correction factor for the acceptor excitation by the donor excitation source (β) using the stoichiometry parameter by displaying FRET efficiency versus stoichiometry (S_{PIE}) in Margarita (Equation 1, below).
   NOTE: β is chosen such that the donor sample has a peak at S_{PIE} = 1.0 in the stoichiometry scale; the acceptor-only sample should have a stoichiometry of S_{PIE} = 0.0, and the dsDNA with both labels should have a stoichiometry of S_{PIE} ~0.5.
   NOTE: Instrument is now ready, and it is possible to measure FRET-labeled samples.
6. Measure and analyze FRET-labeled samples prepared in section 3 by following steps 6.3-6.4.

Representative Results

In typical smFRET experiments using an MFD setup (laser lines: 485 nm at 60 µW and 640 nm at 23 µW, section 5.1), the fluorescence sample is diluted to a low-picomolar concentration (10^{-12} M = 1 pM) and placed in a confocal microscope, where a sub-nanosecond laser pulse excites labeled molecules freely diffusing through an excitation volume. A typical confocal volume is <4 femtoliters (fL). At such low concentrations, only single molecules are detected one at a time. The emitted fluorescence from the labeled molecules is collected through the objective and is spatially filtered using a pinhole. This step defines an effective confocal detection volume. Then, the signal is split into parallel and perpendicular components at two (or more) different spectral windows (*e.g.,* "green" and "red"). Each photon detector channel is then coupled to time-correlated single-photon counting (TCSPC) electronics for data registration (**Figure 1**).

After following the calibration of the MFD setup, a procedure summarized in **Table 1** (steps 5-6), measurement of the dsDNA standards, can be started. Then, PIE-MFD is used to analyze multiple parameters, such as mean macrotime, fluorescence lifetime, burst-integrated anisotropy, ratio of the signal in green over the signal in red, burst duration in the prompt channel ($T_{(G+R)|D}$), burst duration in the delayed channel ($T_{R|A}$), and others[65,66] (**Figure 2**). Important in this analysis is the stoichiometry parameter (S_{PIE}), defined as:

$$S_{PIE} = \frac{F_{R|D} - \beta F_{R|A} - \alpha F_{G|D} + \gamma F_{G|D}}{F_{R|D} - \beta F_{R|A} - \alpha F_{G|D} + \gamma F_{G|D} + F_{R|A}}, (1)$$

where $F_{G|D} = F_D$, $F_{R|D} = F_A$, and $F_{R|A}$ are background-corrected fluorescence intensities[63]. For example, $F_{G|D} = I_{G|D}$ - #B_G#, where $I_{G|D}$ is the detected intensity in the green channel from the donor and #B_G# is the mean background count rate on the green channel. Similar corrections are done for the fluorescence of the acceptor from direct excitation of the acceptor ($F_{R|A}$) and for the sensitized emission of the acceptor ($F_{R|D}$). In Equation 1, α is the correction factor for donor-fluorescence crosstalk into the acceptor channel; β is the correction factor for acceptor excitation by the donor excitation source; and γ, where

$$\gamma = \frac{\Phi_{F,A}}{\Phi_{F,D}} \cdot \frac{g_R}{g_G}, (2)$$

is a function of the donor and acceptor quantum yields, $\Phi_{F,D}$ and $\Phi_{F,A}$, respectively, and of the detection efficiencies on the green and red detectors, g_G and g_R. Using S_{PIE}, it is possible to calibrate the proper instrumental factors, such as α, β, and γ, to satisfy S_{PIE} = 1 for the donor-only labeled sample, S_{PIE} = 0 for the acceptor-only sample, and S_{PIE} = 0.5 for the FRET sample. Alternatively, it is possible to use:

$$\frac{\gamma^{(1)}}{\gamma^{(2)}} = \frac{\left(\frac{1}{S_{PIE}^{(1)}} - 1\right)}{\left(\frac{1}{S_{PIE}^{(2)}} - 1\right)} = \frac{\Phi_{F,A}^{(1)}}{\Phi_{F,A}^{(2)}} \quad (3)$$

to derive the quantum yield of a second sample, given that the quantum yield of one sample ($\Phi_{F,A}^{(A,0)(1)}$) is known and that the $S_{PIE}^{(1)}$ and $S_{PIE}^{(2)}$ are determined from the PIE-MFD experiment. In this case, it is assumed that the quantum yield of the high-FRET dsDNA is 0.32 and the quantum yield of the low-FRET dsDNA is determined. The reason for doing this procedure is because it has been noted that the S_{PIE} is different for both low-FRET and high-FRET samples, even though both have one donor on the same location and only one acceptor, but at different locations. After determining the proper quantum yield of the standard samples, as described in Equation (3), the FRET efficiency (E) versus #$\tau_{D(A)}$#$_f$ and F_D/F_A versus #$\tau_{D(A)}$#$_f$ representations are used for further evaluation. The parametric relationship between the FRET efficiency (E_{static}), F_D/F_A, and #$\tau_{D(A)}$#$_f$ parameters is described by the following set of equations (Equation 4):

$$E_{static} = \left[1 + \frac{\Phi_{F,A}}{\Phi_{F,D}} \cdot \frac{F_{D|D}}{F_{A|D}}\right]^{-1} = 1 - \frac{\langle \tau_{D(A)} \rangle_x}{\tau_D^{(D,0)}}, (4.1)$$

$$\left(\frac{F_{D|D}}{F_{A|D}}\right)_{static} = \left[\frac{\Phi_{F,D}}{\Phi_{F,A}} \cdot \left(\frac{\langle \tau_{D(A)} \rangle_x}{\tau_D^{(D,0)}} - 1\right)\right]^{-1} . (4.2)$$

Here, $F_{D|D}$ is the donor fluorescence detected in the donor or green channel; $F_{A|D}$ is the acceptor-sensitized emission; $\tau_D^{(D,0)}$ is the donor fluorescence lifetime in the absence of the acceptor; and $\#\tau_{D(A)}\#_x$ is the species average lifetime, which is related to the fluorescence average lifetime by an empirical polynomial $\langle \tau_{D(A)} \rangle_x = \sum_{i=0}^{3} \langle \tau_{D(A)} \rangle_f$ [56,57]. These equations are known as the static FRET lines[57,67] because the lines should cross both populations equally well, in the absence of dynamics (**Figure 3**).

Last comes the analysis of FRET efficiency histograms (**Figure 4**) using probability distribution analysis (PDA) for the two dsDNA samples[68,69]. PDA has been used to model the smFRET histograms with high accuracy[57]. The information of single or multi-static species can be obtained from a single histogram. After fitting the shape of the expected distribution to the experimental data obtained, the distance between the donor and acceptor can be revealed. In short, the FRET efficiency, or F_D/F_A distributions, are calculated by first obtaining the probability **[Equation]** of observing a certain combination of photons collected in the "green" (*G*) and "red" (*R*) detection channels given a certain time-window; use Equation 5:

$$P(S_G, S_R) = \sum_{F_G + B_G = S_G;\ F_R + B_R = S_R} P(F)P(F_G, F_R|F)P(B_G)P(B_R) \quad (5)$$

Here, the fluorescence intensity distribution, $P(F)$, is obtained from the total signal intensity distribution $P(S)$, assuming that the background signals B_G and B_R are distributed according to Poisson distributions, $P(B_G)$ and $P(B_R)$, with known mean background count-rate intensities, $\#B_G\#$ and $\#B_R\#$. The conditional probability $P(F_G, F_R|F)$ is the probability of observing a particular combination of green and red fluorescence photons, F_G and F_R, for a given FRET state.

PDA analysis shows that the interdye distance for the high-FRET dsDNA is $\#R_{DA}\#_E^{(HFRET)}$ = 45.7 Å, while for the low-FRET dsDNA, the distance $\#R_{DA}\#_E^{(LFRET)}$ = 59.7 Å. When compared to the expected distances using the FRET positioning and screening system (FPS)[26], an expected interdye distance $\#R_{DA}\#_{E,AV}^{(HFRET)}$ = 44.7 Å was found as derived using FPS for the high-FRET dsDNA and $\#R_{DA}\#_{E,AV}^{(LFRET)}$ = 59.1 Å for the low-FRET dsDNA. AV stands for the accessible volume calculation embedded in the FPS toolkit. AV is a coarse-grained Monte Carlo simulation, where fluorophores represent three radii hard sphere models connected to an attachment point in the biomolecule with a flexible connecting linker[26,57]. A correction for the quantum yield for the low-FRET dsDNA is required, based on the measured S_{PIE}. With these conditions, it is possible to obtain an agreement of ~1 Å between the experimental value and expected value from the AV simulations.

Next, the NMDA GluN1 LBD is measured. The NMDA receptor (NMDAR) is a heteromeric, non-selective cation channel that requires the binding of glycine and glutamate for gating[70]. The LBD, which has a clamshell-like structure, is known to adopt an open clamshell and a closed clamshell-like configuration upon ligand binding based on crystallographic information[71,72]. For MFD experiments, the NMDA GluN1 LBD was mutated at Ser507 and Thr701 (full-length sequence) on opposite sides of the cleft, as has previously been described. It was then labeled using the FRET pair of a cyan-green fluorophore and a far-red fluorophore (see the Materials List), with an R_0 of 52 Å. This construct was used to study the motion of the ligand-binding domain, without the complexity associated with working with a solubilized receptor. Using this construct, at least three configurations of the LBD were found. It was suggested that a conformational selection mechanism selectively populated one of the identified populations upon ligand binding[73]. In the inactivated form, or in the presence of the antagonist 5,7-dichlorokynurenic acid (DCKA), mostly medium- to low-FRET states are explored, with a longer donor fluorescence lifetime and a larger donor-to-acceptor fluorescence ratio peaking at F_D/F_A = 3.3 (**Figure 5A**). This is consistent with the stabilization of an open-cleft conformation. PDA and time window analysis were used to identify three configurations that the LBD can adopt (the high-FRET (HF) ($\#R_{DA}\#_E$ = 33.9 Å), medium-FRET (MF) ($\#R_{DA}\#_E$ = 45.8 Å), and low-FRET states (LF) ($\#R_{DA}\#_E$ = 55.8 Å)). However, mostly the medium-FRET and the low-FRET were populated. This suggests that the high-FRET is the state that leads to the activation of the NMDAR. It is worth noting that experimentally derived distances and those derived by the FPS using *in silico* labeling and using the crystallographic information (Protein Data Bank Identification (PDBID): 1PB7 and 1PBQ) were compared. It was found that the interdye distance for the medium-FRET and low-FRET populations were $\#R_{DA}\#_{E,AV}$ = 48.7 Å and 54.2 Å for both structures, respectively (**Figure 5B**). The largest deviation of 2.9 Å was found in the medium-FRET state. When considering the uncertainty of the distribution, from the assumption of κ^2 = 2/3, there is a maximum error of 2.5% in the measured distance. In short, one can conclude that it is possible to reach Angstrom accuracy on experimentally determined distances.

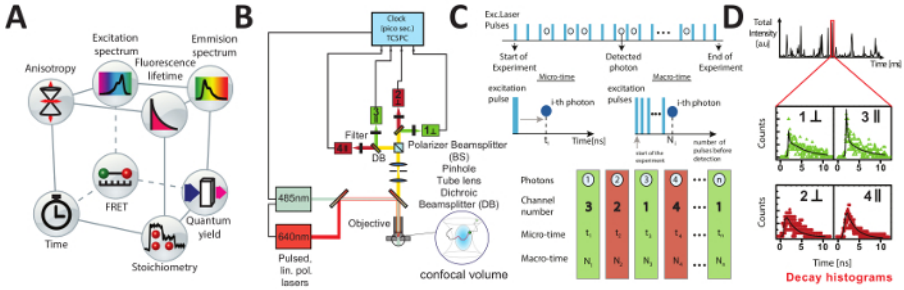

Figure 1: Experimental setup and data registration for PIE-MFD. (**A**) A typical multiparameter fluorescence detection setup is shown and consists of four detectors covering two different spectral windows. Detectors are connected to the time-correlated single-photon counting (TCSPC) electronics. (**B**) In TCSPC, each photon is identified by three parameters: (i) micro-time, or time after the excitation pulse; (ii) macro-time, or the number of excitation pulses from the start of the experiment; and (iii) channel number. These three parameters are required for off-line analysis. (**C**) Single molecules diffuse freely through the confocal volume, and photons are emitted, leaving a burst of photons as a function of time. (**D**) Each selected burst is fitted accordingly and used for displaying multi-dimensional histograms. Please click here to view a larger version of this figure.

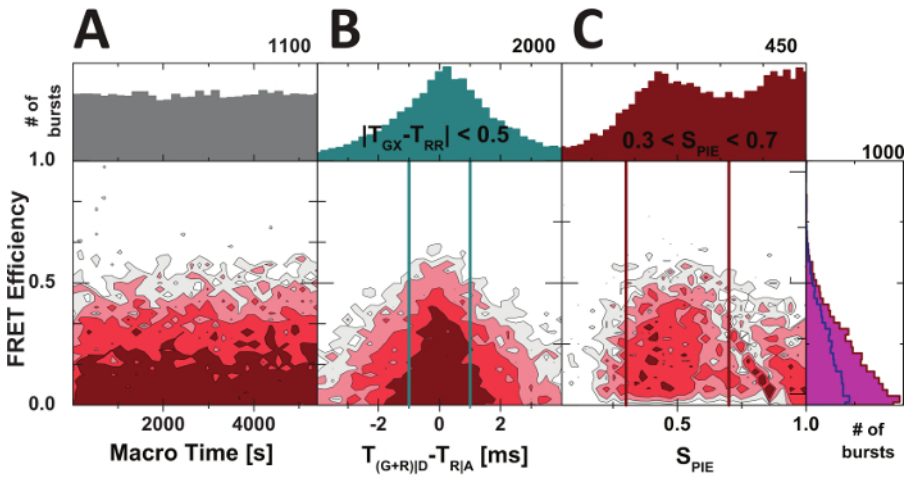

Figure 2: Burst analysis using various fluorescence parameters. (**A**) FRET efficiency versus macrotime, (**B**) FRET efficiency versus $T_{(G+R)|D} - T_{R|A}$, and (**C**) FRET efficiency versus S_{PIE} for the low-FRET or 15 bp dsDNA. $T_{(G+R)|D}$ is the burst duration in the prompt channel, and $T_{R|A}$ is the burst duration in the delayed channel ($T_{R|A}$) Please click here to view a larger version of this figure.

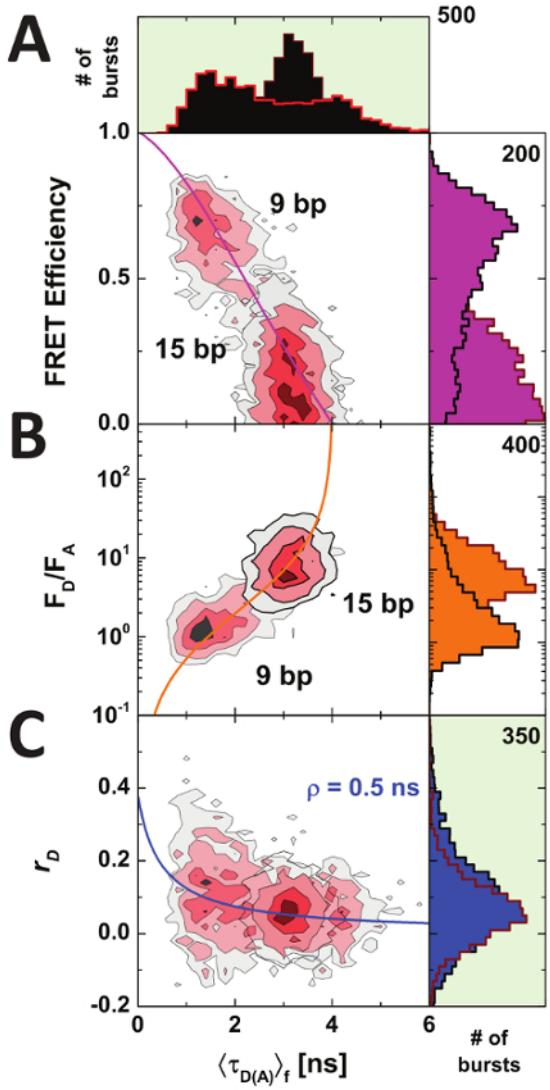

Figure 3: F_D/F_A and lifetime of the donor versus FRET efficiency. Two-dimensional histograms to represent FRET efficiency (**A**); the ratio of donor over acceptor fluorescence, F_D/F_A, (**B**); and donor anisotropy r_D (**C**) versus the average fluorescence lifetime of the donor in the presence of acceptor $\#\tau_{D(A)}\#_f$. The determined correction factors are: $\#B_G\# = 0.64$, $\#B_R\# = 0.37$, $\beta = 0.08$ (the fraction of the direct excitation of the acceptor with the donor excitation laser), $\alpha = 0.017$, and $g_G/g_R = 3.7$ Please click here to view a larger version of this figure.

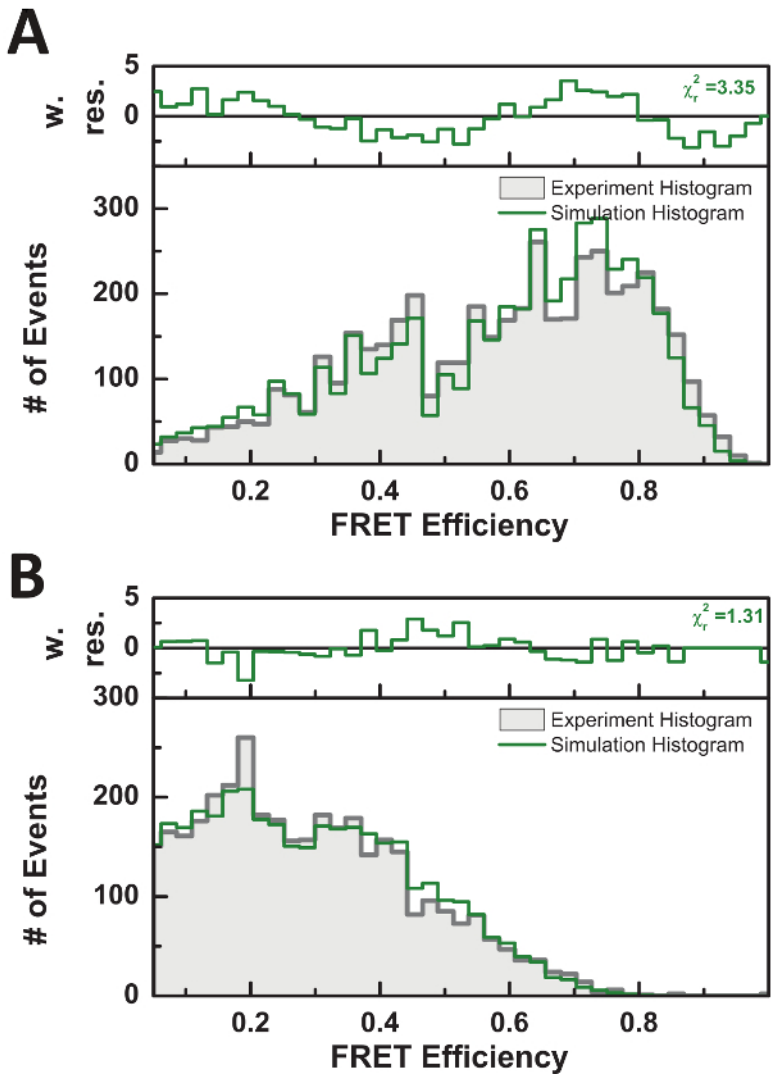

Figure 4: PDA comparisons of high-FRET and low-FRET dsDNA. Time window PDA analysis at 2 ms, with a half-width of 6% of the mean FRET efficiency distance. Each distance is Gaussian distributed with 6% of the $\#R_{DA}\#_E$ as the width (hw_{DA}). (**A**) For the sample HFRET, the interdye distance is $\#R_{DA}\#_E^{(HFRET)}$ = 45.7 Å. (**B**) For the sample LFRET, the distance is $\#R_{DA}\#_E^{(LFRET)}$ = 59.7 Å. Please click here to view a larger version of this figure.

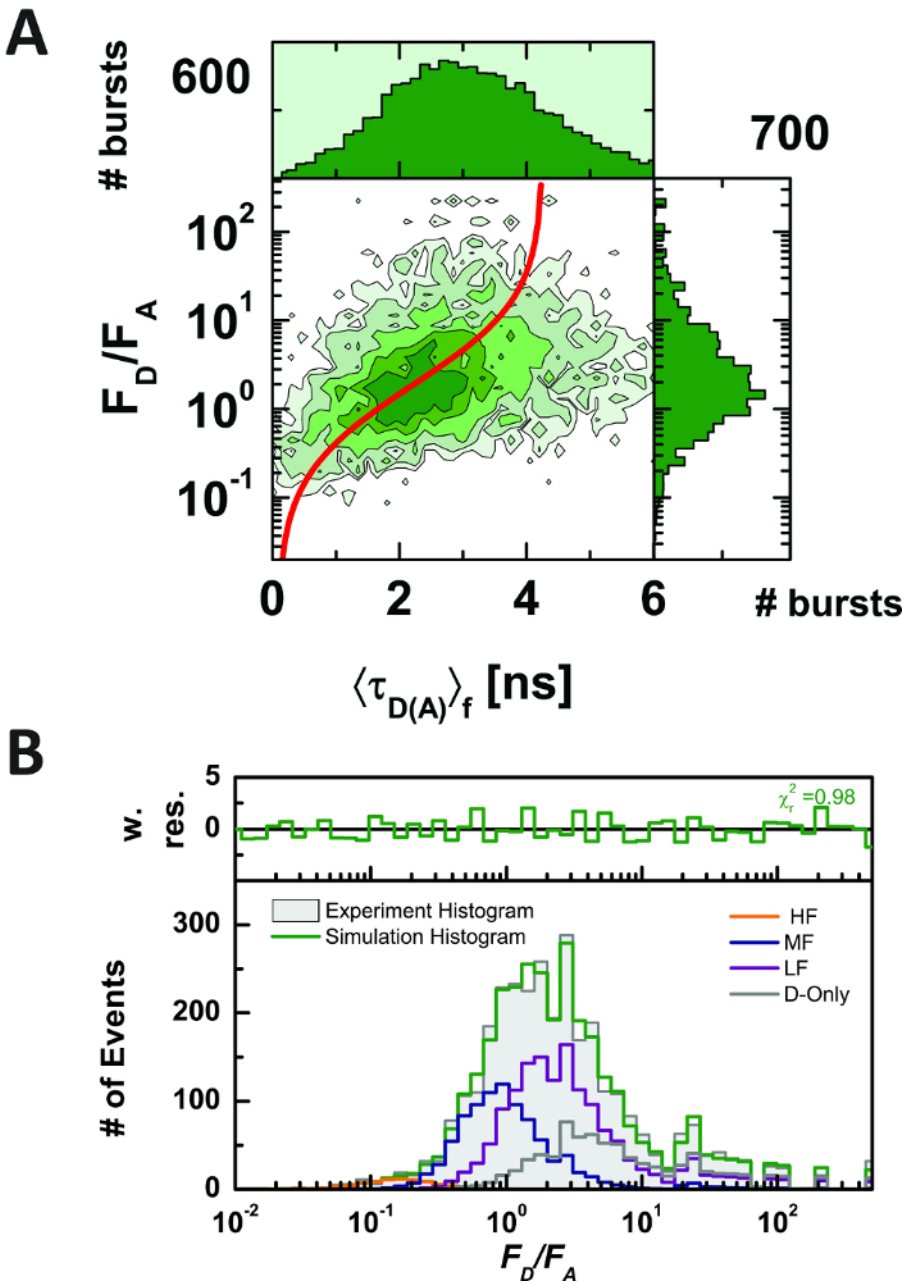

Figure 5: PIE-MFD of the ligand-binding domain of the NMDA receptor in the presence of the antagonist, DCKA. (**A**) Two-dimensional histogram of F_D/F_A versus the lifetime of the donor in the presence of acceptor $\#\tau_{D(A)}\#_f$ and the anisotropy of the donor versus $\#\tau_{D(A)}\#_f$ for the LBD with DCKA. One-dimensional projections for F_D/F_A and are also shown. The static FRET line is shown in red. Pure donor and acceptor fluorescence (F_D and F_A) are corrected for background ($\#B_G\#$ = 0. 940 kHz and $\#B_R\#$ = 0.522 kHz), spectral cross-talk (α = 1.7%), and detection efficiency ratio (g_G/g_R = 3.7). On the anisotropy versus $\#\tau_{D(A)}\#_f$ histograms, the Perrin's equation has a rotational correlation of ρ = 2.5 ns. (**B**) PDA at a 10-ms time window Δt. A single state is needed. The model fits all time windows nicely. Please click here to view a larger version of this figure.

Action	Goal
Center laser beam.	
Align pinhole.	FCS experiment (section 5).
Align detectors.	Maximize CPM.
Adjust objective correction ring.	Minimize t_{diff} and maximize CPM.
Determine instrument response function (IRF).	TCSPC @ SMD in TTTR mode. Measure scatter decay pattern.
Determine G-factor for each spectral window.	TCSPC @ SMD in TTTR mode. Compare intensities form decay tails fitting for polarizations.
Determine detection efficiency ratio in spectral windows (g_R/g_G).	(i) Intensity measurements of a dye with broad emission spectrum (nM concentration). (ii) Measure reference FRET rulers (pM concentration). In MFD the subpopulation should fall on the static FRET line.
Perform final check (lifetime and anisotropy).	Control fitted lifetime and anisotropy from single-molecule measurement of freely diffusing dye with a single exponential decay (*e.g.* Rhodamine 110).
Determine ratio of acceptor over donor quantum yield.	(i) Stoichiometry plot (S_{PIE}) Eq. 1. and 4.2.
Determine background count rate.	Intensity measurements of the selected "buffer".
Determine cross-talk (α).	Intensity measurements of donor dye into account the fluorescence emission spectrum and detection efficiencies.

Table 1: Calibration steps for FRET experiments in single-molecule experiments.

Discussion

In this work, the protocol to align, calibrate, and measure interdye distances with high precision using PIE-MFD single-molecule FRET experiments is presented. By carefully calibrating all instrumental parameters, one can increase the accuracy of the measured distances and reach Angstrom accuracy. To do so, various multidimensional histograms are used to analyze and identify populations for further characterization. Using the mean macro time to verify the stability of the measured samples, it is possible to correct for donor and acceptor photobleaching and to select FRET populations based on the stoichiometry parameter. However, the photophysical properties of the acceptor can change depending on the location of the label. Thus, one can use a S_{PIE} distribution to properly correct for the acceptor quantum yield. Proper photophysical characterization is necessary to determine the gamma factor (γ), which, together with other correction factors (*e.g.,* α for crosstalk and β for acceptor excitation with the donor laser), can be used to increase the accuracy of the measured interdye distance. This approach was corroborated using two designed dsDNA standard samples, and an accuracy of ~1 Å when compared to expected values was determined.

Different dye selections require adapting the microscope optical elements, such as the dichroic and bandpass filters, to accommodate the proper spectral window of the selected dyes. Accordingly, pulsed lasers need to be selected. More importantly, the selection of dyes is crucial because of several possible photophysical artifacts, such as acceptor and donor bleaching, triplet or dye blinking, or dye sticking to protein surfaces. These artifacts could compromise the interpretation of experimental data. MFD is ideal in this scenario because, by inspecting multiple parameters, it is possible to identify the sources of these artifacts, correct for them, or at least be aware of their existence. The dipole orientation parameter, most of the time assumed as $\kappa^2 = 2/3$, can cause larger deviations of the determined distance if the dye sticks preferentially to the surface of the biomolecules. Anisotropy of the donor sample, acceptor sample, and donor acceptor can help to resolve whether this assumption is valid or not. In this experiment, it has been found that there is a maximum error of ~2.5% on the measured distance, compared to not making the proper correction and obtaining a 10-20% error. The quantum yield of the acceptor can create a larger source of error. Thus, S_{PIE} is important for addressing this important issue.

It is possible to apply a similar strategy to understand the conformational landscape of the ligand-binding domain of the NMDA receptor to understand the mechanism of agonism on the NMDAR. It was found that the LBD in the presence of an antagonist shuns the accessibility of a high-FRET state, postulated to be responsible for opening the channel[73]. When comparing experimentally derived distances and the expected values based on crystallographic information, an agreement within 3 Å was achieved. More importantly, the new low-populated states can be identified with similar precision.

In summary, single-molecule FRET experiments in MFD mode[42] allow one to properly account for experimental artifacts and to derive interdye distance in the range of ~30-70 Å. If, instead of a single measured distance, a network of distances is derived, it is possible to use these as restraints in structural modeling, particularly for states that are difficult to characterize with more standard methods of structural biology.

Disclosures

All the authors declare that they have no competing financial interests with the contents of this article.

Acknowledgements

VJ and HS acknowledge support from NIH R01 GM094246 to VJ. HS acknowledges start-up funds from the Clemson University Creative Inquiry Program and the Center for Optical Materials Science and Engineering Technologies at Clemson University. This project was also supported by a training fellowship from the Keck Center for Interdisciplinary Bioscience Training of the Gulf Coast Consortia (NIGMS Grant No. 1 T32GM089657-05) and the Schissler Foundation Fellowship for Translational Studies of Common Human Diseases to DD. The content is solely the responsibility of the authors and does not necessarily represent the official views of the National Institutes of Health.

References

1. Kendrew, J. C. Architecture of a protein molecule. *Nature.* **182** (4638), 764-767 (1958).
2. Kendrew, J. C. *et al.* A three-dimensional model of the myoglobin molecule obtained by x-ray analysis. *Nature.* **181** (4610), 662-666 (1958).
3. Henzler-Wildman, K., & Kern, D. Dynamic personalities of proteins. *Nature.* **450** (7172), 964-972 (2007).
4. Henzler-Wildman, K. A. *et al.* A hierarchy of timescales in protein dynamics is linked to enzyme catalysis. *Nature.* **450** (7171), 913-U927 (2007).
5. Henzler-Wildman, K. A. *et al.* Intrinsic motions along an enzymatic reaction trajectory. *Nature.* **450** (7171), 838-U813 (2007).
6. Kline, A. D., & Wuthrich, K. Secondary structure of the alpha-amylase polypeptide inhibitor tendamistat from Streptomyces tendae determined in solution by 1H nuclear magnetic resonance. *J. Mol. Biol.* **183** (3), 503-507 (1985).
7. Williamson, M. P., Havel, T. F., & Wuthrich, K. Solution conformation of proteinase inhibitor IIA from bull seminal plasma by 1H nuclear magnetic resonance and distance geometry. *J. Mol. Biol.* **182** (2), 295-315 (1985).
8. Havel, T. F., & Wuthrich, K. An evaluation of the combined use of nuclear magnetic resonance and distance geometry for the determination of protein conformations in solution. *J. Mol. Biol.* **182** (2), 281-294 (1985).
9. Förster, T. Zwischenmolekulare Energiewanderung und Fluoreszenz. *Ann.Phys.* **2** 55-75 (1948).
10. Stryer, L., & Haugland, R. P. Energy transfer: a spectroscopic ruler. *Proc Natl Acad Sci U S A.* **58** (2), 719-726 (1967).
11. Schuler, B., Lipman, E. A., Steinbach, P. J., Kumke, M., & Eaton, W. A. Polyproline and the "spectroscopic ruler" revisited with single-molecule fluorescence. *Proc Natl Acad Sci U S A.* **102** (8), 2754-2759 (2005).
12. Wozniak, A. K., Schroder, G. F., Grubmuller, H., Seidel, C. A., & Oesterhelt, F. Single-molecule FRET measures bends and kinks in DNA. *Proc Natl Acad Sci U S A.* **105** (47), 18337-18342 (2008).
13. Orrit, M., & Bernard, J. Single Pentacene Molecules Detected by Fluorescence Excitation in a p-Terphenyl Crystal. *Phys. Rev. Lett.* **65** (21), 2716-2719 (1990).
14. Weiss, S. Fluorescence spectroscopy of single biomolecules. *Science.* **283** (5408), 1676-1683 (1999).
15. Ha, T. *et al.* Probing the interaction between two single molecules: Fluorescence resonance energy transfer between a single donor and a single acceptor. *Proc.Natl.Acad.Sci.USA.* **93** 6264-6268 (1996).
16. Michalet, X., Weiss, S., & Jager, M. Single-molecule fluorescence studies of protein folding and conformational dynamics. *Chem. Rev.* **106** (5), 1785-1813 (2006).
17. Jares-Erijman, E. A., & Jovin, T. M. FRET imaging. *Nat. Biotechnol.* **21** (11), 1387-1395 (2003).
18. Sakon, J. J., & Weninger, K. R. Detecting the conformation of individual proteins in live cells. *Nat Methods.* **7** (3), 203-205 (2010).
19. Stahl, Y. *et al.* Moderation of Arabidopsis root stemness by CLAVATA1 and ARABIDOPSIS CRINKLY4 receptor kinase complexes. *Curr. Biol.* **23** (5), 362-371 (2013).
20. Fessl, T. *et al.* Towards characterization of DNA structure under physiological conditions in vivo at the single-molecule level using single-pair FRET. *Nucleic Acids Res.* **40** (16), e121 (2012).
21. Stryer, L. Fluorescence energy transfer as a spectroscopic ruler. *Annu. Rev. Biochem.* **47** 819-846 (1978).
22. Schuler, B., Lipman, E. A., Steinbach, P. J., Kumke, M., & Eaton, W. A. Polyproline and the "spectroscopic ruler" revisited with single-molecule fluorescence. *Proc. Natl. Acad. Sci. USA.* **102** (8), 2754-2759 (2005).
23. Best, R. B. *et al.* Effect of flexibility and cis residues in single-molecule FRET studies of polyproline. *Proc Natl Acad Sci USA.* **104** (48), 18964-18969 (2007).
24. Hoefling, M. *et al.* Structural heterogeneity and quantitative FRET efficiency distributions of polyprolines through a hybrid atomistic simulation and Monte Carlo approach. *PLoS One.* **6** (5), e19791 (2011).
25. Hellenkamp, B., Wortmann, P., Kandzia, F., Zacharias, M., & Hugel, T. Multidomain structure and correlated dynamics determined by self-consistent FRET networks. *Nat Methods.* (2016).
26. Kalinin, S. *et al.* A toolkit and benchmark study for FRET-restrained high-precision structural modeling. *Nat. Meth.* **9** (12), 1218-1225 (2012).
27. Hickerson, R., Majumdar, Z. K., Baucom, A., Clegg, R. M., & Noller, H. F. Measurement of internal movements within the 30 S ribosomal subunit using Forster resonance energy transfer. *J. Mol. Biol.* **354** (2), 459-472 (2005).
28. Margittai, M. *et al.* Single-molecule fluorescence resonance energy transfer reveals a dynamic equilibrium between closed and open conformations of syntaxin 1. *Proceedings of the National Academy of Sciences.* **100** (26), 15516-15521 (2003).
29. Weninger, K., Bowen, M. E., Chu, S., & Brunger, A. T. Single-molecule studies of SNARE complex assembly reveal parallel and antiparallel configurations. *Proc. Natl. Acad. Sci. USA.* **100** (25), 14800-14805 (2003).
30. Brunger, A. T., Strop, P., Vrljic, M., Chu, S., & Weninger, K. R. Three-dimensional molecular modeling with single molecule FRET. *J. Struct. Biol.* **173** (3), 497-505 (2011).
31. Choi, U. B. *et al.* Single-molecule FRET-derived model of the synaptotagmin 1-SNARE fusion complex. *Nat. Struct. Mol. Biol.* **17** (3), 318-324 (2010).
32. DeRocco, V., Anderson, T., Piehler, J., Erie, D. A., & Weninger, K. Four-color single-molecule fluorescence with noncovalent dye labeling to monitor dynamic multimolecular complexes. *BioTechniques.* **49** (5), 807-816 (2010).
33. McCann, J. J., Zheng, L., Chiantia, S., & Bowen, M. E. Domain orientation in the N-Terminal PDZ tandem from PSD-95 is maintained in the full-length protein. *Structure.* **19** (6), 810-820 (2011).
34. McCann, J. J. *et al.* Supertertiary structure of the synaptic MAGuK scaffold proteins is conserved. *Proc Natl Acad Sci USA.* **109** (39), 15775-15780 (2012).

35. Andrecka, J. *et al.* Nano positioning system reveals the course of upstream and nontemplate DNA within the RNA polymerase II elongation complex. *Nucleic Acids Res.* **37** (17), 5803-5809 (2009).
36. Muschielok, A. *et al.* A nano-positioning system for macromolecular structural analysis. *Nat Methods.* **5** (11), 965-971 (2008).
37. Muschielok, A., & Michaelis, J. Application of the Nano-Positioning System to the Analysis of Fluorescence Resonance Energy Transfer Networks. *J. Phys. Chem. B.* **115** (41), 11927-11937 (2011).
38. Renner, A. *et al.* High Precision FRET Reveals Dynamic Structures in the Drosophila Scaffold Protein Complex Stardust-DPATJ-DLin-7 Mediated by L27 Domains. *Biophys. J.* **106** (2), 256a (2014).
39. Antonik, M., Felekyan, S., Gaiduk, A., & Seidel, C. A. Separating structural heterogeneities from stochastic variations in fluorescence resonance energy transfer distributions via photon distribution analysis. *The Journal of Physical Chemistry B.* **110** (13), 6970-6978 (2006).
40. Gaiduk, A., Kühnemuth, R., Antonik, M., & Seidel, C. A. Optical Characteristics of Atomic Force Microscopy Tips for Single-Molecule Fluorescence Applications. *ChemPhysChem.* **6** (5), 976-983 (2005).
41. Eggeling, C., Fries, J., Brand, L., Günther, R., & Seidel, C. Monitoring conformational dynamics of a single molecule by selective fluorescence spectroscopy. *Proceedings of the National Academy of Sciences.* **95** (4), 1556-1561 (1998).
42. Kudryavtsev, V. *et al.* Combining MFD and PIE for Accurate Single-Pair Förster Resonance Energy Transfer Measurements. *ChemPhysChem.* **13** (4), 1060-1078 (2012).
43. Steven, A. C., & Baumeister, W. The future is hybrid. *J. Struct. Biol.* **163** (3), 186-195 (2008).
44. Cowieson, N. P., Kobe, B., & Martin, J. L. United we stand: combining structural methods. *Curr. Opin. Struct. Biol.* **18** (5), 617-622 (2008).
45. Boura, E. *et al.* Solution structure of the ESCRT-I complex by small-angle X-ray scattering, EPR, and FRET spectroscopy. *Proc Natl Acad Sci USA.* **108** (23), 9437-9442 (2011).
46. Dominguez, C., Boelens, R., & Bonvin, A. M. HADDOCK: a protein-protein docking approach based on biochemical or biophysical information. *J. Am. Chem. Soc.* **125** (7), 1731-1737 (2003).
47. Laible, M., & Boonrod, K. Homemade site directed mutagenesis of whole plasmids. *J Vis Exp.* (27) (2009).
48. Barker, K. *At the Bench: A Laboratory Navigator.* Cold Spring Harbor Laboratory Press (2005).
49. Coleman, J. A., Green, E. M., & Gouaux, E. Thermostabilization, Expression, Purification, and Crystallization of the Human Serotonin Transporter Bound to S-citalopram. *J Vis Exp.* (117), e54792 (2016).
50. Yates, L. A., & Gilbert, R. J. C. Efficient Production and Purification of Recombinant Murine Kindlin-3 from Insect Cells for Biophysical Studies. *J Vis Exp.* (85), e51206 (2014).
51. GE Healthcare. *Protein Sample Preparation, Handbook*. <http://www.gelifesciences.com/file_source/GELS/Service%20and%20Support/Documents%20and%20Downloads/Handbooks/Protein_sample_preparation_handbook.pdf> (2016).
52. Li, Q., Richard, C.-A., Moudjou, M., & Vidic, J. Purification and Refolding to Amyloid Fibrils of (His)6-tagged Recombinant Shadoo Protein Expressed as Inclusion Bodies in E. coli. *J Vis Exp.* (106), e53432 (2015).
53. Scopes, R. K. *Protein Purification: Principles and Practice.* Springer New York, (1993).
54. *Protein Extiction Coefficient Calculator.* <http://www.biomol.net/en/tools/proteinextinction.htm> (2016).
55. GE. *Desalting Column Product booklet.* <https://www.gelifesciences.com/gehcls_images/GELS/Related%20Content/Files/1478781880316/litdoc52130800_20161110134421.pdf> (2016).
56. Lakowicz, J. R. *Principles of Fluorescence Spectroscopy.* Springer US, (2007).
57. Sindbert, S. *et al.* Accurate distance determination of nucleic acids via Forster resonance energy transfer: implications of dye linker length and rigidity. *J. Am. Chem. Soc.* **133** (8), 2463-2480 (2011).
58. Wahl, M. *PicoQuant Technical Note.* <http://www.picoquant.com/technotes/technote_tttr. pdf> (accessed 2010), (2004).
59. Elson, E. L., & Magde, D. Fluorescence correlation spectroscopy. I. Conceptual basis and theory. *Biopolymers.* **13** (1), 1-27 (1974).
60. Magde, D., Elson, E. L., & Webb, W. W. Fluorescence correlation spectroscopy. II. An experimental realization. *Biopolymers.* **13** (1), 29-61 (1974).
61. Felekyan, S. *et al.* Full correlation from picoseconds to seconds by time-resolved and time-correlated single photon detection. *Rev. Sci. Instrum.* **76** (8), 083104 (2005).
62. Iyer, V., Rossow, M. J., & Waxham, M. N. Peak two-photon molecular brightness of fluorophores is a robust measure of quantum efficiency and photostability. *JOSA B.* **23** (7), 1420-1433 (2006).
63. Böhmer, M., Wahl, M., Rahn, H.-J., Erdmann, R., & Enderlein, J. Time-resolved fluorescence correlation spectroscopy. *Chem. Phys. Lett.* **353** (5), 439-445 (2002).
64. Fries, J. R., Brand, L., Eggeling, C., Köllner, M., & Seidel, C. A. M. Quantitative identification of different single molecules by selective time-resolved confocal fluorescence spectroscopy. *The Journal of Physical Chemistry A.* **102** (33), 6601-6613 (1998).
65. Kühnemuth, R., & Seidel, C. A. M. Principles of Single Molecule Multiparameter Fluorescence Spectroscopy. *Single Mol.* **2** (4), 251-254 (2001).
66. Widengren, J. *et al.* Single-molecule detection and identification of multiple species by multiparameter fluorescence detection. *Anal. Chem.* **78** (6), 2039-2050 (2006).
67. Sisamakis, E., Valeri, A., Kalinin, S., Rothwell, P. J., & Seidel, C. A. Accurate single-molecule FRET studies using multiparameter fluorescence detection. *Methods Enzymol.* **475** 455-514 (2010).
68. Kalinin, S., Felekyan, S., Antonik, M., & Seidel, C. A. Probability distribution analysis of single-molecule fluorescence anisotropy and resonance energy transfer. *The Journal of Physical Chemistry B.* **111** (34), 10253-10262 (2007).
69. Kask, P. *et al.* Two-dimensional fluorescence intensity distribution analysis: theory and applications. *Biophys. J.* **78** (4), 1703-1713 (2000).
70. Traynelis, S. F. *et al.* Glutamate Receptor Ion Channels: Structure, Regulation, and Function. *Pharmacol. Rev.* **62** (3), 405-496 (2010).
71. Furukawa, H., & Gouaux, E. Mechanisms of activation, inhibition and specificity: crystal structures of the NMDA receptor NR1 ligand-binding core. *EMBO J.* **22** (12), 2873-2885 (2003).
72. Furukawa, H., Singh, S. K., Mancusso, R., & Gouaux, E. Subunit arrangement and function in NMDA receptors. *Nature.* **438** (7065), 185-192 (2005).
73. Dolino, D. M., Rezaei Adariani, S., Shaikh, S. A., Jayaraman, V., & Sanabria, H. Conformational Selection and Submillisecond Dynamics of the Ligand-binding Domain of the N-Methyl-d-aspartate Receptor. *J. Biol. Chem.* **291** (31), 16175-16185 (2016).

